NUCL SCI TECH (2018) 29:90
https://doi.org/10.1007/s41365-018-0422-0

A density functional theory study on the interaction between UO_2^{2+} and the carbamoylphosphoramidic acid ligand for uranium extraction from seawater

Xiao-Jing Guo[1] · Cheng Li[1] · Jiang-Tao Hu[1] · Hong-Juan Ma[1] · Hong-Liang Qian[2]

Received: 22 August 2017 / Revised: 16 November 2017 / Accepted: 4 December 2017 / Published online: 9 May 2018

Abstract Phosphorylurea molecules, which contain both phosphoryl and carbonyl groups, are considered efficient extractants for UO_2^{2+}. This study aims to explain the complexation of UO_2^{2+} with carbamoylphosphoramidic acid (CPO), a simple model for phosphorylurea, for ligand design for uranium recovery from seawater using density functional theory calculations, natural bond order analysis, and the quantum theory of atoms in molecules. The results showed that, when CPO acts as a monodentate ligand, the affinity of phosphoryl for UO_2^{2+} is stronger than that of carbonyl, and CPO coordinates with UO_2^{2+} through the phosphoryl oxygen atom. When CPO serves as a bidentate ligand, both the phosphoryl and carbonyl oxygen atoms connect to UO_2^{2+}, and the U–O(carbonyl) bond plays a more important role than the U–O(phosphoryl) bond in the interaction between UO_2^{2+} and CPO. This paradox may be caused by the significant charge transfer from the U–O(carbonyl) π bond orbital to the C–N σ antibond orbital of the bidentate CPO. The NH spacer between the phosphoryl and carbonyl groups could ensure the delocalization of the electron system of the molecule. The bidentate binding motif is favored by entropy and opposed by enthalpy, while the monodentate binding motif is favored by enthalpy and opposed by entropy. Ultimately, the bidentate binding motif is more favorable than the monodentate one. As expected, the interaction between UO_2^{2+} and the deprotonated CPO is stronger than that between UO_2^{2+} and the neutral CPO. Comparing the interaction between UO_2^{2+} and CPO with that between UO_2^{2+} and *N*-phenylcarbamoylphosphoramidic acid (PhCPO), formed by replacing one hydrogen atom from the terminal nitrogen atom of CPO with a phenyl group, the phenyl substituent at the terminal nitrogen atom of PhCPO shows a slightly negative effect on the interaction between UO_2^{2+} and PhCPO.

Keywords Uranium extraction · Adsorption · Density functional theory

1 Introduction

Concerns about the energy crisis and greenhouse gas emissions prompted more and more countries to choose nuclear power as a clean energy source [1, 2]. Nuclear energy provides over 11% of the world's electricity as a continuous and reliable base-load power, without carbon dioxide emission. Uranium consumption is expected to continue to rise to meet the increasing nuclear energy demands in the foreseeable future. Provided that all uranium mines currently under development enter service as

---

Electronic supplementary material The online version of this article (https://doi.org/10.1007/s41365-018-0422-0) contains supplementary material, which is available to authorized users.

This work was supported by the National Natural Science Foundation of China (Nos. 21676291, 21406272, 21571185, and 11605273), the Shanghai Sailing Program (No. 16YF1408500), and the Jiangsu Planned Projects for Postdoctoral Research Funds (No. 1402060B).

✉ Xiao-Jing Guo
guoxiaojing@sinap.ac.cn

✉ Hong-Liang Qian
hlqian@cpu.edu.cn

[1] Shanghai Institute of Applied Physics, Chinese Academy of Sciences, Shanghai 201800, China

[2] School of Engineering, China Pharmaceutical University, Nanjing 210009, China

planned, the uranium market should be adequately supplied just until 2025 according to the World Nuclear Association report. However, we could extend that by 6500 years if half of the uranium resources (estimated at 4.5 billion tons) in the ocean could be recovered [3].

Ligand design is a very important field in the development of effective adsorbents for uranium recovery from seawater. Phosphoryl-containing compounds show high affinity for UO_2^{2+}. It has been reported that uranyl phosphates and arsenates constitute about one-third of the ~ 200 known uranium minerals [4]. This truly proves the strong affinity of phosphoryl for uranium. Phosphonate ligands are currently used to extract uranium in the TRUEX (transuranic extraction) and PUREX (plutonium and uranium recovery by extraction) processes [5, 6]. Several researchers such as Alexandratos et al. [7] and Yuan et al. [8] have also pointed out the high affinity of phosphonate ligands for UO_2^{2+}. Another proof of the strong affinity of phosphoryl for UO_2^{2+} is the higher uranium sorption capacity of phosphoric acid-functionalized mesoporous carbon sorbents compared to amidoxime-functionalized materials, which are known to be efficient for uranium extraction from seawater [9]. Moreover, carbonyl could also bind to UO_2^{2+}; therefore, both the phosphoryl- and carbonyl-containing ligands have been incorporated into mesoporous materials to be used as sorbents for UO_2^{2+} [9, 10].

Bidentate organophosphorous compounds containing both phosphoryl and carbonyl are considered efficient extractants for UO_2^{2+}; for example, carbamoylphosphine oxide (CMPO) is well known and often used in the TRUEX process [11]. The predominant connecting site of CMPO with UO_2^{2+} is the phosphoryl oxygen (OP) atom, while the carbonyl oxygen (OC) atom can connect with a proton and serve as an internal buffer [12]. Wang et al. [13] reported that CMPO coordinated as a bidentate chelating ligand through both the OP and OC atoms for 1:1-type complexes, and as monodentate ligand interacting with UO_2^{2+} through the OP atoms for 2:1-type complexes [13]. The *N*-diphenylphosphorylurea ligand, another group containing both phosphoryl and carbonyl, has also been shown to effectively bind to UO_2^{2+} [1, 14]. Similar in structure to CMPO, phosphorylurea molecules have a NH spacer between the phosphoryl and carbonyl groups as opposed to the CH_2 spacer in the CMPO ligands. It has been said that the CH_2 spacer between the phosphoryl and carbonyl groups in a CMPO molecule does not ensure the electronic interactions between them, while replacing CH_2 with NH could ensure the delocalization of the electron system of the molecule to strengthen its affinity for UO_2^{2+} [15]. Moreover, the replacement of CH_2 by NH makes the structure more rigid, and the resulting distances between the OP and OC atoms in phosphorylureas are shorter than those in the corresponding CMPOs, which probably enhance the binding abilities of phosphorylureas for UO_2^{2+} [15].

While there are numerous studies about CMPOs, the interactions between UO_2^{2+} and phosphorylureas have not been fully explored in the literature yet. Matrosov et al. [14] proposed a bidentate binding motif for uranyl complexes with phosphorylureas, while Carboni et al. [1] proposed a monodentate coordination motif where UO_2^{2+} interacts with the OP atom. Additionally, replacing the alkyls at the phosphorous atom with aryls could alter the binding abilities of CMPOs for UO_2^{2+}. It has been previously reported that replacing alkyls at the phosphorous atom with aryls in the CMPO series could enhance the binding abilities of the compounds [15]. Wang et al. [13] reported that the CMPO and diphenyl-*N*,*N*-diisobutylcarbamoyl phosphine oxide (Ph_2CPMO) ligands showed comparable U–ligand binding strengths. What if aryls connect to the terminal nitrogen atom? Since phosphorylureas containing phenyl at the terminal nitrogen atom have been incorporated into mesoporous materials intended as sorbents for UO_2^{2+} [1, 9], more detailed knowledge of the interactions between UO_2^{2+} and phosphorylureas is needed. The information could help advance the disclosing of the structure–property relationships for ligand design for uranium recovery from seawater by showing the effects of electronic and structural differences on binding.

In this research, the binding of UO_2^{2+} with carbamoylphosphoramidic acid (CPO), a simple phosphorylurea model (Fig. 1), as well as *N*-phenylcarbamoylphosphoramidic acid (PhCPO) (Fig. 1) was quantified by applying density functional theory (DFT) calculations. We focused on the stable structures, their bonding characteristics, and the relative stabilities of various uranyl complexes. The difference in calculated properties was interpreted in terms of the electronic and structural differences between various uranyl complexes. Based on the results, we explained the following: (1) which is the interacting site of CPO with UO_2^{2+}, and why, (2) what are the roles of the U–OP and U–OC bonds in the

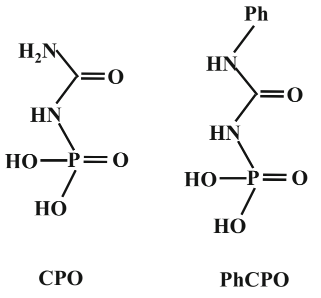

Fig. 1 Molecular skeletons of carbamoylphosphoramidic acid (CPO) and *N*-phenylcarbamoylphosphoramidic acid (PhCPO)

interaction between UO_2^{2+} and CPO, and (3) whether the binding strength of UO_2^{2+} with CPO is affected by incorporating a phenyl group into CPO at the terminal nitrogen atom.

2 Computational methods

We performed DFT calculations using the Gaussian-09 C1 package [16] at the B3LYP level of theory [17, 18]. The spin–orbit coupling effects were not considered during the calculations. The Stuttgart RSC 1997 effective core potential (ECP) was used for uranium. This potential includes the 60 electrons in the core for uranium atoms to take scalar relativistic effects into consideration. The remaining 32 electrons are described by the associated valence basis set [19–21]. It has been reported that the additional diffuse functions to the oxygen and hydrogen atoms can significantly affect the U, d, f, and p populations of $(UO_2)_2(OH)_2(H_2O)_6^{2+}$, while the additional polarization function does not [22]. Diffuse functions are very important and often necessary to use when negatively charged ligands are involved [23]. Additionally, for the complexes with phenyl rings, dispersion effects must be non-negligible. Therefore, in this paper, we used the 6-31++G* basis set for carbon, nitrogen, oxygen, and hydrogen atoms. This level of theory accurately yields the main features of actinyl complexes [13, 24, 25]. No symmetry constraint was applied during the calculations. Harmonic vibrational frequency calculations at the same level verified that each structure was a minimum with zero imaginary frequency. As discussed in our previous papers, aqueous environments influence the binding motif of the relatively stable isomers for some uranyl complexes [26, 27]. Moreover, since we were interested in the structural information for uranyl complexes with CPO and PhCPO in solution, all the structures were fully optimized with solvation effects, via a polarizable conductor calculation model (CPCM), similar to the conductor-like screening model (COSMO) method [28, 29] using the "SCRF = COSMO" keyword in the Gaussian 09 program package. NBO analysis [30] was performed using the NBO 6.0 program [31]. QTAIM analysis [32] was employed to analyze the U–ligand bonds using the Multiwfn 3.3.5 software [33].

The extent of protonation/deprotonation in aqueous solution was determined by the acid dissociation constant (pK_a). We directly calculated the pKa of CPO using the above computational methods, but at a higher basis set of 6-311++G(d, p).

The pK_a for the $CPO \rightleftharpoons DCPO^- + H^+$ reaction is given by:

$$pK_a = \frac{\Delta G^*_{aq}}{2.303RT} = \frac{G^*_{aq,DCPO^-} + G^*_{aq,H^+} - G^*_{aq,CPO}}{2.303RT}, \quad (1)$$

where $G^*_{aq,CPO}$ and $G^*_{aq,DCPO^-}$ are the standard free energy of CPO and deprotonated CPO (DCPO) in aqueous solutions, respectively. The free energy of a proton in aqueous medium is calculated as:

$$G^*_{aq,H^+} = G^\circ_{g,H^+} + \Delta G^*_{aq,H^+} + \Delta G^{1atm\rightarrow 1M}, \quad (2)$$

where $G^\circ_{g,H^+} = H^\circ_{g,H^+} - TS^\circ_{g,H^+}$ is the gas-phase free energy of the proton at 298.15 K obtained using $H^\circ_{g,H^+} = \frac{5RT}{2} = 1.48\,\mathrm{kcal/mol}$ and

$$S^\circ_{g,H^+} = 26.05\mathrm{cal/(mol \cdot K)} \cdot \Delta G^*_{aq,H^+} = -265.9\mathrm{kcal/mol}$$

is the aqueous-phase solvation free energy of the proton, as reported in the literature [34–36]. $\Delta G^{1atm\rightarrow 1M}$ is a correction term for the change in the standard state of 1 atm to 1 mol/L, calculated as $RT\log(24.4) = 1.89\mathrm{kcal/mol}$. The symbols * and ° refer to the standard state: 1 mol/L and 1 atm, respectively.

Also, the pK_a for the $DCPO^- \rightleftharpoons DDCPO^{2-} + H^+$ reaction is given by:

$$pK_a = \frac{\Delta G^*_{aq}}{2.303\,RT} = \frac{G^*_{aq,DDCPO^{2-}} + G^*_{aq,H^+} - G^*_{aq,DCPO^-}}{2.303\,RT}, \quad (3)$$

where $G^*_{aq,DCPO^-}$ and $G^*_{aq,DDCPO^{2-}}$ are the standard free energy of DCPO and deprotonated DCPO (DDCPO) in aqueous solution, respectively.

The effect of explicit water on the calculated pK_a's was assessed by adding two explicit water molecules hydrogen-bonded directly to the site being protonated/deprotonated as shown in Fig. 2.

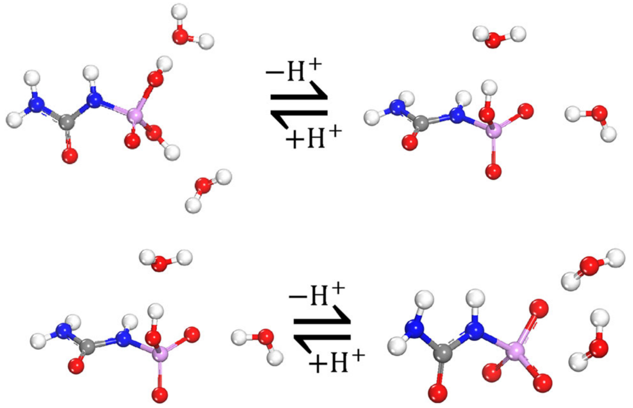

Fig. 2 (Color online) Arrangement of the explicit water molecules near the OH and O^- groups in CPO

3 Results and discussion

UO_2^{2+} is known to coordinate with five water molecules forming a pentahydrate complex $[UO_2(H_2O)_5]^{2+}$ in aqueous solution. Since the literature about the structures of uranyl complexes with CPO is scarce, we optimized $UO_2(H_2O)_5^{2+}$ and $UO_2(CO_3)_3^{4-}$ in aqueous solution to check the reliability of our theoretical methods (see Figure S1 and Table S1). Additionally, using similar methods and calculation setups, we recently studied the coordination of uranyl hydrates [37] and successfully predicted the structures of uranyl complexes with amine, amidoximate, and carboxyl groups both in gas phase and aqueous solution [26, 27]. The structural properties after optimization agree well with other calculation results and experiments [38–40].

When UO_2^{2+} interacts with CPO/PhCPO, aqua groups are added to the equatorial plane of UO_2^{2+}, resulting in a penta-coordinated pattern in the equatorial plane of UO_2^{2+}. As stated in Introduction section, both phosphoryl and carbonyl show affinity for UO_2^{2+}. CPO/PhCPO could serve as a monodentate ligand coordinating with UO_2^{2+} through either the OP or OC atom referred to as binding motifs I and II. In addition, both the OP and OC atoms could bind to UO_2^{2+} forming a bidentate binding motif referred to as III. Therefore, $[UO_2(H_2O)_4(L)]^{2+}$ containing monodentate ligands and $[UO_2(H_2O)_3(L)]^{2+}$ containing bidentate ligands were studied as 1:1 ligand/metal stoichiometric complexes (where L=CPO or PhCPO, hereinafter), while $[UO_2(H_2O)_3(L)_2]^{2+}$ containing two monodentate ligands, $[UO_2(H_2O)_2(L)_2]^{2+}$ containing one monodentate and one bidentate ligand, and $[UO_2(H_2O)(L)_2]^{2+}$ containing two bidentate ligands were studied as 2:1 ligand/metal stoichiometric complexes. Moreover, the corresponding complexes with deprotonated CPO or PhCPO: $[UO_2(H_2O)_4(DL)]^{+}$, $[UO_2(H_2O)_3(DL)]^{+}$, $[UO_2(H_2O)_3(DL)_2]$, $[UO_2(H_2O)_2(DL)_2]$, and $[UO_2(H_2O)(DL)_2]$ were investigated (DL=DCPO or DPhCPO, and represent the deprotonated CPO or PhCPO, hereinafter).

3.1 Structural and vibrational properties

3.1.1 Complexes with 1:1 ligand/metal stoichiometry

Table 1 Calculated U=O, U–OP, and U–OC distances (Å) of most energetically stable, **a** $[UO_2(H_2O)_4(L)]^{2+}$ and $[UO_2(H_2O)_3(L)]^{2+}$ (L=CPO or PhCPO) and **b** $[UO_2(H_2O)_4(DL)]^{+}$ and $[UO_2(H_2O)_3(DL)]^{+}$ (DL=DCPO or DPhCPO). OP and OC represent the phosphoryl and carbonyl oxygen atoms

	$[UO_2(H_2O)_4(L)]^{2+}$		$[UO_2(H_2O)_3(L)]^{2+}$	
	L=CPO	L=PhCPO	L=CPO	L=PhCPO
(a)				
U=O	1.767	1.767	1.769	1.768
U–OP	2.343	2.355	2.380	2.396
U–OC	–	–	2.353	2.368
	$[UO_2(H_2O)_4(DL)]^{+}$		$[UO_2(H_2O)_3(DL)]^{+}$	
	DL=DCPO	DL=DPhCPO	DL=DCPO	DL=DPhCPO
(b)				
U=O	1.774	1.773	1.775	1.774
U–OP	2.260	2.260	2.303	2.306
U–OC	–	–	2.352	2.361

According to the optimized geometries and zero-point energies for $[UO_2(H_2O)_4(L)]^{2+}$ in Figure S2(a), binding motif I is favored over II. This indicates that the electron-donating ability of the OP atom is stronger than that of the OC atom. Figure 3a presents the most energetically stable geometries of $[UO_2(H_2O)_4(L)]^{2+}$ where the monodentate ligands coordinate with UO_2^{2+} through the OP atoms and $[UO_2(H_2O)_3(L)]^{2+}$ for the 1:1 ligand/metal stoichiometric complexes. As shown in Table 1a, the U–O(CPO) distances are slightly shorter than the U–O(PhCPO) distances for $[UO_2(H_2O)_4(L)]^{2+}$ and $[UO_2(H_2O)_3(L)]^{2+}$, which indicates that the interaction between UO_2^{2+} and CPO is slightly stronger than that between UO_2^{2+} and PhCPO. These results also imply that the phenyl substituent at the terminal nitrogen atom of PhCPO shows a slightly negative effect on the interaction between UO_2^{2+} and PhCPO. It is generally known that the donation of electrons to the U center by the equatorial ligands weakens the U=O bond. The U=O bond lengths for uranyl complexes with CPO are almost the same as those for the complexes with PhCPO, which indicates that the charge transfers from equatorial ligands to the U centers for uranyl complexes with CPO and PhCPO are similar. The calculated symmetric and asymmetric vibrational frequencies of uranyl for the most energetically stable $[UO_2(H_2O)_4(L)]^{2+}$ and $[UO_2(H_2O)_3(L)]^{2+}$ are presented in Table 2a. The stronger U=O bonds are accompanied by higher uranyl stretching vibrational frequencies. In accordance with the U=O bond lengths, the uranyl stretching vibrational frequencies for uranyl complexes with CPO and PhCPO are similar. These results indicate that the phenyl substitute at the terminal nitrogen atom has an insignificant effect on the binding ability of PhCPO for UO_2^{2+}. Specifically, for $[UO_2(H_2O)_3(L)]^{2+}$, the distances between U and the OP atoms of the bidentate ligands are longer than those between U and the OC atoms. These results indicate that the U–OC bonds play a more important role than the U–OP bonds in the interactions between UO_2^{2+} and the bidentate CPO/PhCPO. This is opposite to the fact that the electron-

Table 2 Calculated frequencies (cm^{-1}) of the symmetrical and asymmetrical stretching modes of U=O for the most energetically stable (a) $[UO_2(H_2O)_4(L)]^{2+}$ and $[UO_2(H_2O)_3(L)]^{2+}$ (L=CPO or PhCPO) and (b) $[UO_2(H_2O)_4(DL)]^{+}$ and $[UO_2(H_2O)_3(DL)]^{+}$ (DL=DCPO or DPhCPO)

	$[UO_2(H_2O)_4(L)]^{2+}$		$[UO_2(H_2O)_3(L)]^{2+}$	
	Asym	Sym	Asym	Sym
(a)				
L=CPO	953	897	948	892
L=PhCPO	953	895	950	891
	$[UO_2(H_2O)_4(DL)]^{+}$		$[UO_2(H_2O)_3(DL)]^{+}$	
	Asym	Sym	Asym	Sym
(b)				
DL=DCPO	938	872	932	873
DL=DPhCPO	938	872	934	874

donating abilities of the OP atoms are stronger than those of the OC atoms for CPO/PhCPO, which will be discussed in Sect. 3.3.

The calculated pK_{a1} and pK_{a2} values for CPO are 1.49 and 13.59, respectively, while the pK_{a1} and pK_{a2} values become 1.87 and 12.26 when two explicit water molecules are added near the OH and O^- groups in CPO as shown in Fig. 2. According to the pK_a values, CPO could very likely lose one proton forming DCPO in seawater, while DDCPO is difficult to form. Thus, we also studied the uranyl complexes with DCPO and DPhCPO. In addition, according to the optimized geometries and zero-point energies in Figure S3a, binding motif I is favored over II for $[UO_2(H_2O)_4(DL)]^{+}$. The most energetically stable geometries of $[UO_2(H_2O)_4(DL)]^{+}$ where the monodentate ligands coordinate to UO_2^{2+} through the OP atoms and $[UO_2(H_2O)_3(DL)]^{+}$ with binding motif III are presented in Fig. 3b. As shown in Tables 1b and 2b, the U=O bond lengths and the uranyl stretching vibrational frequencies for the uranyl complexes with DCPO and DPhCPO are very similar. The U–O (DCPO/DPhCPO) distances are all shorter than the corresponding U–O (CPO/PhCPO) distances, while the U=O bond lengths for uranyl complexes with DCPO/DPhCPO are longer than the corresponding values for uranyl complexes with CPO/PhCPO as shown in Table 1. Additionally, uranyl stretching vibrational frequencies decrease with the deprotonation of CPO/PhCPO (Table 2). These results indicate that the interactions of UO_2^{2+} with DCPO/DPhCPO are stronger than those with CPO/PhCPO. It is reasonable to assume that positively charged UO_2^{2+} interacts strongly with the negatively charged DCPO/DPhCPO compared with the neutral CPO/PhCPO. According to the distances between U and the oxygen atoms of the bidentate DCPO/DPhCPO, the U–OP bonds play a more important role than the U–OC bonds in the interactions between UO_2^{2+} and the bidentate DCPO/DPhCPO for $[UO_2(H_2O)_3(DL)]^{+}$. This is different for $[UO_2(H_2O)_3(L)]^{2+}$ where the U–OC bonds play a leading role in the interactions between UO_2^{2+} and the bidentate CPO/PhCPO since the deprotonation of CPO/PhCPO causes more electrons to gather at the phosphoryl group, thus causing the bonds between U and the OP atoms of DCPO/DPhCPO to be stronger.

3.1.2 Complexes with 2:1 ligand/metal stoichiometry

Three kinds of 2:1 ligand/metal stoichiometric uranyl complexes, $[UO_2(H_2O)_3(L)_2]^{2+}$, $[UO_2(H_2O)_2(L)_2]^{2+}$, and $[UO_2(H_2O)(L)_2]^{2+}$, were examined. The two ligands (CPO or PhCPO) bind to UO_2^{2+} in a monodentate style for $[UO_2(H_2O)_3(L)_2]^{2+}$ and serve as bidentate ligands for $[UO_2(H_2O)(L)_2]^{2+}$. While one ligand coordinates to UO_2^{2+} in binding motif I, the other acts as a bidentate ligand for $[UO_2(H_2O)_2(L)_2]^{2+}$. Similar to the case of uranyl complexes with 1:1 ligand/metal stoichiometry, binding motif I

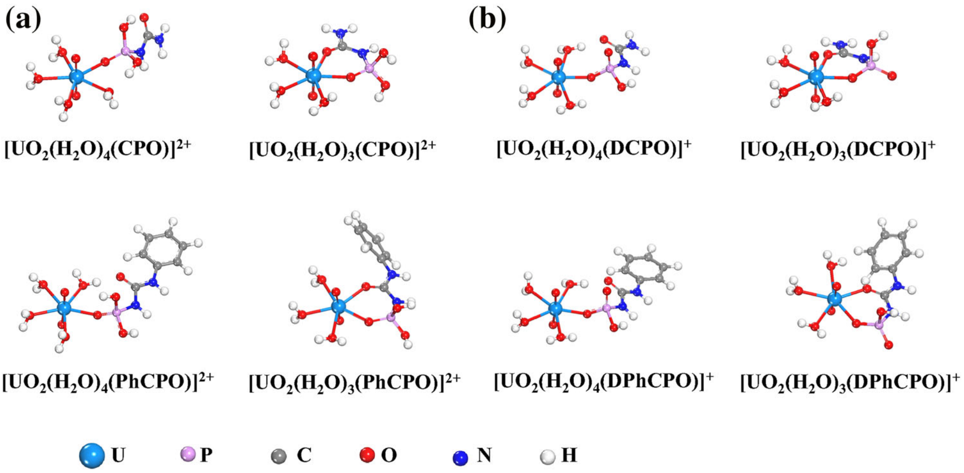

$[UO_2(H_2O)_4(CPO)]^{2+}$ $[UO_2(H_2O)_3(CPO)]^{2+}$ $[UO_2(H_2O)_4(DCPO)]^{+}$ $[UO_2(H_2O)_3(DCPO)]^{+}$

$[UO_2(H_2O)_4(PhCPO)]^{2+}$ $[UO_2(H_2O)_3(PhCPO)]^{2+}$ $[UO_2(H_2O)_4(DPhCPO)]^{+}$ $[UO_2(H_2O)_3(DPhCPO)]^{+}$

Fig. 3 (Color online) Optimized structures of most energetically stable, **a** $[UO_2(H_2O)_4(L)]^{2+}$ and $[UO_2(H_2O)_3(L)]^{2+}$ (L=CPO or PhCPO) and **b** $[UO_2(H_2O)_4(DL)]^{+}$ and $[UO_2(H_2O)_3(DL)]^{+}$ (DL=DCPO or DPhCPO) is favored over II for uranyl complexes with 2:1 ligand/metal stoichiometry according to the optimized geometries and zero-point energies for $[UO_2(H_2O)_3(L)_2]^{2+}$ and $[UO_2(H_2O)_2(L)_2]^{2+}$ in Figure S2c and d. Figure 4a presents the most energetically stable geometries of $[UO_2(H_2O)_3(L)_2]^{2+}$, $[UO_2(H_2O)_2(L)_2]^{2+}$, and $[UO_2(H_2O)(L)_2]^{2+}$. The monodentate CPO/PhCPO coordinates with UO_2^{2+} through the OP atoms, which proves again that the electron-donating ability of the OP atom is stronger than that of the OC atom of CPO and PhCPO. As shown in Table 3a, the distances between U and the oxygen atoms of monodentate CPO and PhCPO are very similar for $[UO_2(H_2O)_3(L)_2]^{2+}$ and $[UO_2(H_2O)_2(L)_2]^{2+}$. The U–OP and U–OC bonds between UO_2^{2+} and the bidentate CPO are shorter than the corresponding bonds between UO_2^{2+} and the bidentate PhCPO for $[UO_2(H_2O)_2(L)_2]^{2+}$, while the U–OP bonds between UO_2^{2+} and the bidentate CPO are longer than those between UO_2^{2+} and the bidentate PhCPO for $[UO_2(H_2O)(L)_2]^{2+}$. These might be explained by the numerous hydrogen bonds between the hydrogen atoms of CPO/PhCPO and the oxygen atoms of H_2O in the equatorial plane of uranyl. Additionally, the U=O bond lengths for $[UO_2(H_2O)_3(CPO)_2]^{2+}$, $[UO_2(H_2O)_2(CPO)_2]^{2+}$, and $[UO_2(H_2O)(CPO)_2]^{2+}$ are almost the same as those for $[UO_2(H_2O)_3(PhCPO)_2]^{2+}$, $[UO_2(H_2O)_2(PhCPO)_2]^{2+}$, and $[UO_2(H_2O)(PhCPO)_2]^{2+}$, respectively, which indicates that the charge transfer from the equatorial ligands to the U centers for uranyl complexes with CPO and PhCPO are similar. The calculated frequencies of the symmetrical and asymmetrical stretching modes of U=O for the most energetically stable $[UO_2(H_2O)_3(L)_2]^{2+}$, $[UO_2(H_2O)_2(L)_2]^{2+}$, and $[UO_2(H_2O)(L)_2]^{2+}$ are presented in Table 4a. Similarly to the case of uranyl complexes with 1:1 ligand/metal stoichiometry, the uranyl stretching vibrational frequencies for uranyl complexes with CPO and PhCPO are comparable for $[UO_2(H_2O)_3(L)_2]^{2+}$, $[UO_2(H_2O)_2(L)_2]^{2+}$,

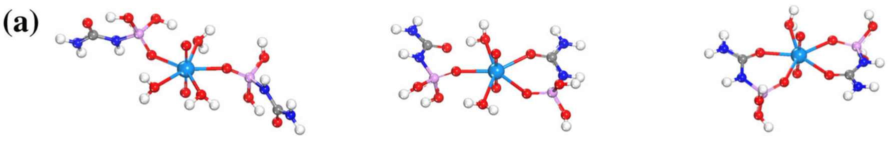

$[UO_2(H_2O)_3(CPO)_2]^{2+}$ $[UO_2(H_2O)_2(CPO)_2]^{2+}$ $[UO_2(H_2O)(CPO)_2]^{2+}$

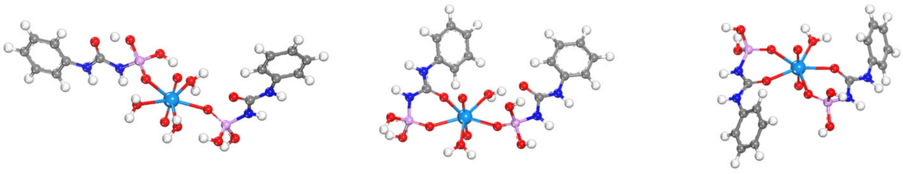

$[UO_2(H_2O)_3(PhCPO)_2]^{2+}$ $[UO_2(H_2O)_2(PhCPO)_2]^{2+}$ $[UO_2(H_2O)(PhCPO)_2]^{2+}$

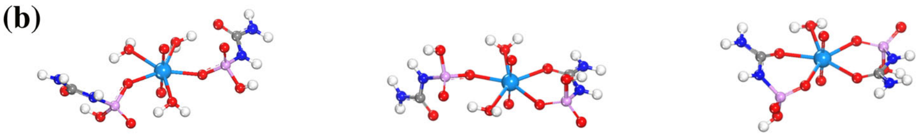

$[UO_2(H_2O)_3(DCPO)_2]$ $[UO_2(H_2O)_2(DCPO)_2]$ $[UO_2(H_2O)(DCPO)_2]$

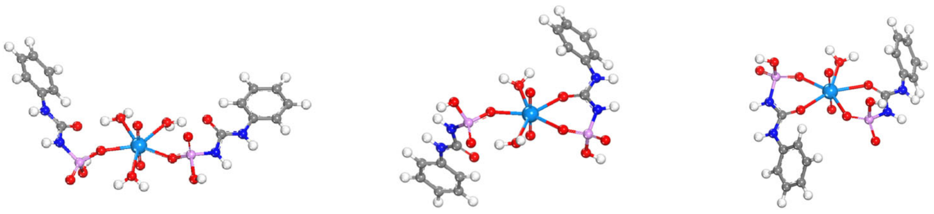

$[UO_2(H_2O)_3(DPhCPO)_2]$ $[UO_2(H_2O)_2(DPhCPO)_2]$ $[UO_2(H_2O)(DPhCPO)_2]$

● U ● P ● C ● O ● N ● H

Fig. 4 (Color online) Optimized structures of most energetically stable, **a** $[UO_2(H_2O)_3(L)_2]^{2+}$, $[UO_2(H_2O)_2(L)_2]^{2+}$, and $[UO_2(H_2O)(L)_2]^{2+}$ (L=CPO or PhCPO) and **b** $[UO_2(H_2O)_3(DL)_2]$, $[UO_2(H_2O)_2(DL)_2]$, and $[UO_2(H_2O)(DL)_2]$ (DL=DCPO or DPhCPO)

Table 3 Calculated U=O, U–OP, and U–OC distances (Å) for the most energetically stable (a) $[UO_2(H_2O)_3(L)_2]^{2+}$, $[UO_2(H_2O)_2(L)_2]^{2+}$, and $[UO_2(H_2O)(L)_2]^{2+}$ (L=CPO or PhCPO) and (b) $[UO_2(H_2O)_3(DL)_2]$, $[UO_2(H_2O)_2(DL)_2]$, and $[UO_2(H_2O)(DL)_2]$ (DL=DCPO or DPhCPO)

	$[UO_2(H_2O)_3(L)_2]^{2+}$		$[UO_2(H_2O)_2(L)_2]^{2+}$		$[UO_2(H_2O)(L)_2]^{2+}$	
	L=CPO	L=PhCPO	L=CPO	L=PhCPO	L=CPO	L=PhCPO
(a)						
U=O	1.768	1.766	1.772	1.771	1.773	1.773
U–OP1[a]	2.353	2.356	2.378	2.374	2.423	2.403
U–OC1[a]					2.382	2.386
U–OP2[a]	2.348	2.342	2.416	2.420	2.412	2.399
U–OC2[a]			2.371	2.390	2.390	2.395
	$[UO_2(H_2O)_3(DL)_2]$		$[UO_2(H_2O)_2(DL)_2]$		$[UO_2(H_2O)(DL)_2]$	
	L=DCPO	L=DPhCPO	L=DCPO	L=DPhCPO	L=DCPO	L=DPhCPO
(b)						
U=O	1.781	1.781	1.781	1.781	1.783	1.782
U–OP1[a]	2.321	2.309	2.332	2.339	2.360	2.352
U–OC1[a]					2.384	2.394
U–OP2[a]	2.303	2.298	2.339	2.335	2.342	2.338
U–OC2[a]			2.395	2.405	2.408	2.425

OP and *OC* denote the phosphoryl and carbonyl oxygen atoms

Table 4 Calculated frequencies (cm^{-1}) of the symmetrical and asymmetrical stretching modes of U=O for the most energetically stable (a) $[UO_2(H_2O)_3(L)_2]^{2+}$, $[UO_2(H_2O)_2(L)_2]^{2+}$, and $[UO_2(H_2O)(L)_2]^{2+}$ (L=CPO or PhCPO) and (b) $[UO_2(H_2O)_3(DL)_2]$, $[UO_2(H_2O)_2(DL)_2]$, and $[UO_2(H_2O)(DL)_2]$ (DL=DCPO or DPhCPO)

	$[UO_2(H_2O)_3(L)_2]^{2+}$		$[UO_2(H_2O)_2(L)_2]^{2+}$		$[UO_2(H_2O)(L)_2]^{2+}$	
	Asym	Sym	Asym	Sym	Asym	Sym
(a)						
L=CPO	948	887	940	884	938	879
L=PhCPO	954	893	941	881	937	878
	$[UO_2(H_2O)_3(DL)_2]$		$[UO_2(H_2O)_2(DL)_2]$		$[UO_2(H_2O)(DL)_2]$	
	Asym	Sym	Asym	Sym	Asym	Sym
(b)						
L=DCPO	918	853	917	857	912	855
L=DPhCPO	914	848	919	856	914	853

and $[UO_2(H_2O)(L)_2]^{2+}$, which indicates that the phenyl substitute at the terminal nitrogen atom of PhCPO shows only an insignificant effect on the binding ability of PhCPO for uranyl. Specifically, the U–OP bonds are longer than the U–OC bonds between UO_2^{2+} and the bidentate CPO/PhCPO for $[UO_2(H_2O)_2(L)_2]^{2+}$ and $[UO_2(H_2O)(L)_2]^{2+}$. These results indicate that the U–OC bonds play a more important role than the U–OP bonds in the interactions between UO_2^{2+} and the bidentate CPO/PhCPO.

Moreover, UO_2^{2+} binds to the monodentate DCPO/DPhCPO through the OP atoms in binding motif I for $[UO_2(H_2O)_3(DL)_2]$ and $[UO_2(H_2O)_2(DL)_2]$ (Figure S3c, d). The most energetically stable geometries of $[UO_2(H_2O)_3(DL)_2]$, $[UO_2(H_2O)_2(DL)_2]$, and $[UO_2(H_2O)(DL)_2]$ are presented in Fig. 4b. As shown in Table 3b, the U=O bond lengths for uranyl complexes with DCPO and DPhCPO are very similar, and so are the uranyl stretching vibrational frequencies in Table 4b. As expected, the interactions between UO_2^{2+} and DCPO/DPhCPO are stronger than those between UO_2^{2+} and CPO/PhCPO according to the U–O and U=O bond lengths in Table 3 and the uranyl stretching vibrational frequencies in Table 4. Comparing the U–OP and U–OC bond lengths, we can conclude that the U–OP bonds play a more important role than the U–OC bonds in the interactions between UO_2^{2+} and the bidentate DCPO/DPhCPO for $[UO_2(H_2O)_2(DL)_2]$ and $[UO_2(H_2O)(DL)_2]$. These results are in accordance with the results for the uranyl complexes with 1:1 ligand/metal stoichiometry.

3.2 Thermodynamic properties

3.2.1 *Complexes with 1:1 ligand/metal stoichiometry*

Changes in the enthalpies (Δ*H*) and Gibbs free energies (Δ*G*) that accompany the formation of uranyl complexes with 1:1 ligand/metal stoichiometry are listed in Table 5. The energies are calculated based on the most energetically stable geometries for uranyl complexes. As shown in Table 5a, the Δ*H* and Δ*G* values that accompany the formation of $UO_2(H_2O)_4(CPO)^{2+}$ and $UO_2(H_2O)_3(CPO)^{2+}$ are slightly more negative than those accompanying the formation of $UO_2(H_2O)_4(PhCPO)^{2+}$ and $UO_2(H_2O)_3(PhCPO)^{2+}$, respectively, which indicates that the phenyl substituent on the terminal nitrogen atom of PhCPO exerts a slightly negative effect on the interaction between UO_2^{2+} and PhCPO. Additionally, in batch experiments, the steric hindrance effect on uranyl adsorption with PhCPO-functionalized materials could be stronger than that on uranyl adsorption with CPO-functionalized materials. The Δ*G* values for the complexation reactions between uranyl and CPO/PhCPO are negative for the formation of $UO_2(H_2O)_3(L)^{2+}$ and positive for $UO_2(H_2O)_4(L)^{2+}$. These results indicate that the bidentate binding motif is favored over the monodentate one, which is consistent with the results of Matrosov et al. [14]. However, the results are different than those of Carboni et al. [9] obtained based on enthalpies. Specifically, comparing the Δ*H* and Δ*G* values, the entropy exerts a negative effect on the interaction between uranyl and monodentate CPO/PhCPO for $UO_2(H_2O)_4(L)^{2+}$ and a positive effect on the interaction between uranyl and bidentate CPO/PhCPO for $UO_2(H_2O)_3(L)^{2+}$. The entropy was also suggested to play a significant role in the complexation of uranyl with the $H_2PO_4^-$ anion where the complexation was favored by entropy and opposed by enthalpy [41].

The Δ*H* and Δ*G* values for the complexation reactions between uranyl and DCPO/DPhCPO in Table 5b also indicate that binding motif III is favored by entropy and opposed by enthalpy, while binding motif I is opposed by entropy and favored by enthalpy. As expected, the deprotonated ligands show a higher affinity for UO_2^{2+} than the neutral ones. The attachment of phenyl at the terminal nitrogen atom brings a slightly negative effect on the interaction between UO_2^{2+} and DCPO.

3.2.2 *Complexes with 2:1 ligand/metal stoichiometry*

Based on the most energetically stable geometries of uranyl complexes with 2:1 ligand/metal stoichiometry, we collected the Δ*H* and Δ*G* values for the formation of $[UO_2(H_2O)_3(L)_2]^{2+}$, $[UO_2(H_2O)_2(L)_2]^{2+}$, and $[UO_2(H_2O)(L)_2]^{2+}$ (L=CPO or PhCPO) in Table 6a. The Δ*H* values that accompany the formation of $[UO_2(H_2O)_3(CPO)_2]^{2+}$, $[UO_2(H_2O)_2(CPO)_2]^{2+}$, and $[UO_2(H_2O)(CPO)_2]^{2+}$ are negative, while those accompanying the formation of $[UO_2(H_2O)_3(PhCPO)_2]^{2+}$, $[UO_2(H_2O)_2(PhCPO)_2]^{2+}$, and $[UO_2(H_2O)(PhCPO)_2]^{2+}$ are positive. The Δ*G* values are negative if the forming complexes contain bidentate ligands ($UO_2(H_2O)_2(L)_2^{2+}$ and $UO_2(H_2O)(L)_2^{2+}$); however, they are positive for ($UO_2(H_2O)_3(L)^{2+}$). Based on these results, we could reach the same conclusions we reached for uranyl complexes with 1:1 ligand/metal stoichiometry. First, the phenyl substituent on the terminal nitrogen atom of PhCPO exerts a slightly negative effect on the binding strengths of $[UO_2(H_2O)_3(PhCPO)_2]^{2+}$, $[UO_2(H_2O)_2(PhCPO)_2]^{2+}$, and $[UO_2(H_2O)(PhCPO)_2]^{2+}$. Second, the entropy causes a negative effect on the interactions between UO_2^{2+} and the monodentate CPO/PhCPO, while it gives a positive effect on the interactions between UO_2^{2+} and the bidentate CPO/PhCPO.

The Δ*H* and Δ*G* values that accompany the formation of $[UO_2(H_2O)_3(DL)_2]$, $[UO_2(H_2O)_2(DL)_2]$, and

Table 5 Calculated changes in enthalpies and Gibbs free energies (Δ*H* and Δ*G*, kcal/mol) that accompany the formation of (a) $[UO_2(H_2O)_4(L)]^{2+}$ and $[UO_2(H_2O)_3(L)]^{2+}$ (L=CPO or PhCPO) and (b) $[UO_2(H_2O)_4(DL)]^+$ and $[UO_2(H_2O)_3(DL)]^+$ (DL=DCPO or DPhCPO) at 298.15 K

	Δ*H*		Δ*G*	
	L=CPO	L=PhCPO	L=CPO	L=PhCPO
(a)				
$UO_2(H_2O)_5^{2+} + L \rightarrow UO_2(H_2O)_4(L)^{2+} + H_2O$	− 3.4	2.0	1.3	3.3
$UO_2(H_2O)_5^{2+} + L \rightarrow UO_2(H_2O)_3(L)^{2+} + 2H_2O$	− 2.3	1.0	− 7.8	− 5.0
	Δ*H*		Δ*G*	
	L=DCPO	L=DPhCPO	L=DCPO	L=DPhCPO
(b)				
$UO_2(H_2O)_5^{2+} + DL^- \rightarrow UO_2(H_2O)_4(DL)^+ + H_2O$	− 15.0	− 12.7	− 12.0	− 9.3
$UO_2(H_2O)_5^{2+} + DL^- \rightarrow UO_2(H_2O)_3(DL)^+ + 2H_2O$	− 15.9	− 13.1	− 22.3	− 17.3

Table 6 Calculated changes in enthalpies and Gibbs free energies (ΔH and ΔG, kcal/mol) that accompany the formation of (a) $[UO_2(H_2O)_3(L)_2]^{2+}$, $[UO_2(H_2O)_2(L)_2]^{2+}$, and $[UO_2(H_2O)(L)_2]^{2+}$ (L=CPO or PhCPO) and (b) $[UO_2(H_2O)_3(DL)_2]$, $[UO_2(H_2O)_2(DL)_2]$, and $[UO_2(H_2O)(DL)_2]$ (DL=DCPO or DPhCPO) at 298.15 K

	ΔH		ΔG	
	L=CPO	L=PhCPO	L=CPO	L=PhCPO
(a)				
$UO_2(H_2O)_5^{2+} + 2L \rightarrow UO_2(H_2O)_3(L)_2^{2+} + 2H_2O$	−5.7	1.4	2.2	7.8
$UO_2(H_2O)_5^{2+} + 2L \rightarrow UO_2(H_2O)_2(L)_2^{2+} + 3H_2O$	−4.5	1.3	−3.7	−0.8
$UO_2(H_2O)_5^{2+} + 2L \rightarrow UO_2(H_2O)(L)_2^{2+} + 4H_2O$	−3.7	2.8	−13.9	−8.6

	ΔH		ΔG	
	L=DCPO	L=DPhCPO	L=DCPO	L=DPhCPO
(b)				
$UO_2(H_2O)_5^{2+} + 2DL^- \rightarrow UO_2(H_2O)_3(DL)_2 + 2H_2O$	−27.0	−22.4	−19.6	−13.6
$UO_2(H_2O)_5^{2+} + 2DL^- \rightarrow UO_2(H_2O)_2(DL)_2 + 3H_2O$	−25.8	−21.3	−29.0	−22.6
$UO_2(H_2O)_5^{2+} + 2DL^- \rightarrow UO_2(H_2O)(DL)_2 + 4H_2O$	−27.9	−22.1	−40.1	−32.2

$[UO_2(H_2O)(DL)_2]$ (DL=DCPO or DPhCPO) are summarized in Table 6b. Considering all the calculation results, we could reach several conclusions. First, binding motif III is favored over I, and binding motif I is favored over II for uranyl complexes with CPO/PhCPO. In addition, binding motif III is favored by entropy and opposed by enthalpy, while binding motif I is opposed by entropy and favored by enthalpy. Second, the attachment of phenyl at the terminal nitrogen atom exerts a slightly negative effect on the interactions between UO_2^{2+} and PhCPO. Lastly, as expected, the deprotonated ligands show a higher affinity for uranyl than the neutral ligands.

3.3 Electronic structures

3.3.1 Natural bond orbital (NBO) analysis

As discussed above, binding motif I is favored over II for uranyl complexes with CPO/PhCPO, which indicates that the electron-donating ability of the OP atom is stronger than that of the OC atom. Paradoxically, for the complexes showing binding motif III where the bidentate CPO/PhCPO coordinate with UO_2^{2+} through both the OP and OC atoms, the distance between U and the OP atom is longer than that between U and the OC atom, which indicates that the U–OC bonds play a more important role than the U–OP bonds in the interactions between UO_2^{2+} and the bidentate CPO/PhCPO. In order to provide insights into the bonding nature of the U center with the OP and OC atoms, NBO analysis was conducted to investigate the natural charges, Wiberg bond indices (WBIs) [42], donor–acceptor charge transfer, and hybridization of the U–O bonds in the complexes of interest. First, the natural charges of the free and bonded ligands in Table S2 are used to calculate the charge transfer (ΔQ) from the ligands to UO_2^{2+} and the adjacent water molecules as shown in Table 7. As expected, similarly with the interaction energies, the bidentate ligands in $[UO_2(H_2O)_3(L)]^{2+}$ with binding motif III lose more electrons than the monodentate ligands in $[UO_2(H_2O)_4(L)]^{2+}$ with binding motifs I and II. Comparing the WBIs of the U–O bonds in Table 7, the U–OP bonds in $[UO_2(H_2O)_4(L)]^{2+}$ with motif I show a higher degree of covalent character than the U–OC bonds in $[UO_2(H_2O)_4(L)]^{2+}$ with motif II. For $[UO_2(H_2O)_3(L)]^{2+}$, the WBIs of the U–OC bonds are larger than those of the U–OP bonds, which indicates that the U–OC bonds show a higher degree of covalent character than the U–OP bonds, and the U–OC bonds play a more important role than the U–OP bonds in the interactions between UO_2^{2+} and the bidentate CPO/PhCPO.

Second, the second-order perturbation energies ($E^{(2)}$) corresponding to the donor–acceptor charge transfer in complexes larger than 5 kcal/mol are listed in Table 8. The OP atom is a stronger electron donor than the OC atom. This is reflected in the smaller U–OP distance in $[UO_2(H_2O)_4(L)]^{2+}$ with motif I compared to the U–OC distance in $[UO_2(H_2O)_4(L)]^{2+}$ with motif II. The $E^{(2)}$ corresponding to the charge transfer from the lone pairs of OP to the U orbitals are larger than those from the lone pairs of OC. Specifically, there are significant charge transfers from the BD (1) U–OP orbital to the BD*(1) P–N orbital in $[UO_2(H_2O)_4(L)]^{2+}$ with motif I and from the BD (1) U–OC orbital to the BD*(1) N–C orbital in $[UO_2(H_2O)_4(L)]^{2+}$ with motif II. The corresponding $E^{(2)}$ values are 7.16 and 11.02 kcal/mol, respectively. The weaker charge transfer from the BD (1) U–OP orbital to the BD*(1) P–N orbital compared to that from the BD (1) U–OC orbital to the BD*(1) N–C orbital is compensated by the stronger charge transfer from the lone pairs of OP compared to that from the lone pairs of OC to the U orbitals for $[UO_2(H_2O)_4(L)]^{2+}$. Altogether, the charge transfer between the U center

Table 7 Charge transfer (ΔQ) from ligands to UO_2^{2+} and adjacent water molecules and Wiberg bond indices (WBIs) of U–OP and U–OC bonds for uranyl complexes with 1:1 ligand/metal stoichiometry showing different binding motifs

	$[UO_2(H_2O)_4(L)]^{2+}$, motif I		$[UO_2(H_2O)_4(L)]^{2+}$, motif II		$[UO_2(H_2O)_3(L)]^{2+}$, motif III	
	L=CPO	L=PhCPO	L=CPO	L=PhCPO	L=CPO	L=PhCPO
ΔQ	0.297	0.375	0.331	0.354	0.496	0.505
U–OP[a]	0.545	0.462	–	–	0.403	0.390
U–OC[a]	–	–	0.5000	0.475	0.446	0.455

OP and OC denote the phosphoryl and carbonyl oxygen atoms

Table 8 (a) Donor and acceptor orbitals, and the stabilization interaction energies $E^{(2)}$ (kcal/mol). (b) The hybrid atomic orbitals of the U–O bonds for uranyl complexes with 1:1 ligand/metal stoichiometry showing different binding motifs

Donor	Acceptor	$E^{(2)}$ (kcal/mol)
$[UO_2(H_2O)_4(L)]^{2+}$ L=CPO, motif I		
LP (1) OP	LV (3) U	9.67
LP (2) OP	LV (3) U	9.80
BD (1) U–OP	BD*(1) P– N	7.16
LP (1) OP	BD*(1) U–O	7.32
$[UO_2(H_2O)_4(L)]^{2+}$ L=CPO, motif II		
LP (1) OC	RY (1) U	13.87
LP (1) OC	BD*(1) U–O	6.14
BD (1) U–OC	BD*(1) N–C	11.02
$[UO_2(H_2O)_3(L)]^{2+}$ L=CPO, motif III		
LP (1) OP	LV (2) U	6.37
LP (1) OP	LV (3) U	5.00
LP (1) OP	BD*(1) U–O	9.48
LP (1) OC	LV (2) U	9.93
LP (1) OC	LV (3) U	5.03
LP (1) OC	BD*(1) U–O	5.10
BD (2) U–OC	BD*(1) C–N	11.83

OP and OC denote the phosphoryl and carbonyl oxygen atoms

BD bonding orbital; *BD** antibonding orbital; *LP* lone pair; *RY* Rydberg orbital; *LV* lone vacancy

For BD and BD*, (1) and (2) are the σ and π orbitals, respectively

and CPO/PhCPO in $[UO_2(H_2O)_4(L)]^{2+}$ with binding motif I is stronger than that in $[UO_2(H_2O)_4(L)]^{2+}$ with binding motif II. As for $[UO_2(H_2O)_3(L)]^{2+}$ with a bidentate CPO/PhCPO, the $E^{(2)}$ corresponding to the charge transfer from the lone pairs of OP to the U orbitals are slightly larger than that from the lone pairs of OC to the U orbitals. Moreover, there is a significant charge transfer from the BD (2) U–OC orbital to the BD*(1) C–N orbital, and the corresponding $E^{(2)}$ is 11.83 kcal/mol. However, there is no other $E^{(2)}$ corresponding to the charge transfer involving the OP orbital higher than the chosen 5 kcal/mol threshold. This may be the reason for the stronger U–OC bond compared to the U–OP bond in $[UO_2(H_2O)_3(L)]^{2+}$ containing a bidentate CPO/PhCPO ligand.

The hybrid form in Table 9 also offers some hints. For example, in $[UO_2(H_2O)_3(L)]^{2+}$ with a bidentate CPO/PhCPO ligand, the U–OP bond contains 7% uranium character, composed of 52% 6d orbital and 28% 5f orbital, while the U–OC bond contains 8% uranium character, composed of 52% 6d orbital and 29% 5f orbital. These results indicate that the uranium character of the U–OC bond is stronger than that of the U–OP bond, and the contribution of the 6d/5f orbitals to the U–OC bond is also higher than that to the U–OP bond in $[UO_2(H_2O)_3(L)]^{2+}$ with a bidentate CPO ligand, while the contribution of the 6d/5f orbitals to the U–OC bond in $[UO_2(H_2O)_4(L)]^{2+}$ with motif II is lower than that to the U–OP bond in $[UO_2(H_2O)_4(L)]^{2+}$ with motif I.

3.3.2 *Quantum theory of atoms in molecules*

Quantum theory of atoms in molecules is a useful tool for studying the interactions between atoms in a molecule based on electron densities and properties at the bond critical point (BCP) [36]. BCP is the (3, − 1) saddle point on the electron density curvature being a minimum in the direction of the atomic interaction line and maximum in the two directions perpendicular to it. Based on the values of electron densities and their Laplacians at BCPs,

Table 9 Hybrid atomic orbitals of U–OP and U–OC bonds for uranyl complexes with 1:1 ligand/metal stoichiometry showing different binding motifs

	U–OP	U–OC
$[UO_2(H_2O)_4(L)]^{2+}$ L=CPO, motif I	92%O + 8%U U: 50% 6d, 37% 5f	–
$[UO_2(H_2O)_4(L)]^{2+}$ L=CPO, motif II	92%O + 8%U U: 50% 6d, 36% 5f	–
$[UO_2(H_2O)_3(L)]^{2+}$ L=CPO, motif III	93%O + 7%U U: 52% 6d, 28% 5f	92%O + 8%U U: 52% 6d, 29% 5f

OP and OC denote the phosphoryl and carbonyl oxygen atoms interactions can be divided into shared (covalent bonds) and closed shell interactions (ionic bonds, hydrogen bonds, and van der Waals interactions). The electron densities at BCP $\rho(r)$ larger than 0.1 eÅ^{-3} and the large negative Laplacians represent shared interactions, while $\rho(r)$ in the 0.001–0.040 eÅ^{-3} range and small positive Laplacians indicate closed shell interactions [43].

The electron densities and their Laplacians for the critical points of U–OC and U–OP bonds are shown in Table 10. In all cases, the Laplacian is positive, which indicates closed shell interactions. The U–OP bond in $[UO_2(H_2O)_4(L)]^{2+}$ (L=CPO, motif I) has a larger $\rho(r)$ value, and a less positive value of the Laplacian than the U–OC bond in $[UO_2(H_2O)_4(L)]^{2+}$ (L=CPO, motif II) indicates that the U–OP bond shows a higher degree of covalent character for $[UO_2(H_2O)_4(L)]^{2+}$ (L=CPO, motif I) compared to the U–OC bond for $[UO_2(H_2O)_4(L)]^{2+}$ (L=CPO, motif II). Depending on the values of the electron densities and their Laplacians at BCPs, the U–OP bond shows a lower degree of covalent character than the U–OC bond for $[UO_2(H_2O)_3(L)]^{2+}$ (L=CPO, motif III). These results are consistent with the U–O bond lengths and NBO analysis results.

3.4 Substitution reactions between $UO_2(CO_3)_3^{4-}$ and CPO

As uranium in seawater mainly exists as the very stable uranyl tri-carbonate complex, we also studied the coordination of substitution complexes from $UO_2(CO_3)_3^{4-}$ and CPO. The geometry with monodentate binding motif was identified to be energetically more stable than the geometry with bidentate binding motif for $[UO_2(CO_3)_2(CPO)]^{2-}$ (substitution complex with 1:1 ligand/U stoichiometry). $[UO_2(CO_3)_2(CPO)_2]^{2-}$ and $[UO_2(CO_3)(CPO)_2]^{2-}$ correspond to complexes with 2:1 ligand/U stoichiometry. All the optimized structures for $[UO_2(CO_3)_2(CPO)_2]^{2-}$ and $[UO_2(CO_3)(CPO)_2]^{2-}$ are depicted in Figure S4, and the relatively stable isomers are presented in Fig. 5. $[UO_2(CO_3)_2(CPO)_2]^{2-}$ is a six-coordinated complex with two monodentate CPO ligands. One CPO acts as monodentate ligand, and the other serves as bidentate ligand in $[UO_2(CO_3)(CPO)_2]^{2-}$. The ΔG values for the substitution reactions leading to $[UO_2(CO_3)_2(CPO)]^{2-}$, $[UO_2(CO_3)_2(CPO)_2]^{2-}$, and $[UO_2(CO_3)(CPO)_2]^{2-}$ are all positive, as shown in Table 11. These results indicate that $[UO_2(CO_3)_2(CPO)]^{2-}$, $[UO_2(CO_3)_2(CPO)_2]^{2-}$, and $[UO_2(CO_3)(CPO)_2]^{2-}$ are difficult to form from $UO_2(CO_3)_3^{4-}$ and CPO in aqueous solution at 298.15 K. Also, CPO shows weaker coordinating ability to uranyl than CO_3^{2-}.

As shown above, CPO could very likely deprotonate in seawater. We further examined the substitution reactions from $UO_2(CO_3)_3^{4-}$ and CPO leading to the formation of $[UO_2(CO_3)_2(DCPO)]^{3-}$, $[UO_2(CO_3)_2(DCPO)_2]^{4-}$, and $[UO_2(CO_3)(DCPO)_2]^{2-}$. All optimized geometries are presented in Figure S5, and the relatively stable isomers are shown in Fig. 5. $[UO_2(CO_3)_2(DCPO)]^{3-}$ shows a monodentate binding motif with DCPO coordinating with UO_2^{2+} through the OP atoms. $[UO_2(CO_3)_2(DCPO)_2]^{4-}$ and $[UO_2(CO_3)(DCPO)_2]^{2-}$ are six- and five-coordinated complexes, respectively. The calculated changes in the Gibbs free energy for the substitution reactions leading to $[UO_2(CO_3)_2(DCPO)]^{3-}$ and $[UO_2(CO_3)(DCPO)_2]^{2-}$ are negative as shown in Table 11. This implies that CPO could deprotonate to replace CO_3^{2-} in $UO_2(CO_3)_3^{4-}$ to form $[UO_2(CO_3)_2(DCPO)]^{3-}$ and $[UO_2(CO_3)(DCPO)_2]^{2-}$. $[UO_2(CO_3)_2(DCPO)_2]^{4-}$ is thermodynamically unfavorable in the reaction between $[UO_2(CO_3)_2(DCPO)]^{3-}$ with CPO mainly due to steric hindrance.

Table 10 Electron densities ($\rho(r)$, eÅ^{-3}) and Laplacians of the electron densities ($\nabla^2\rho(r)$, eÅ^{-5}) for the selected bond critical points for uranyl complexes with 1:1 ligand/metal stoichiometry showing different binding motifs

Complex	Bond	$\rho(r)$	$\nabla^2\rho(r)$
$[UO_2(H_2O)_4(L)]^{2+}$ L=CPO, motif I	OP–U	0.069	0.287
$[UO_2(H_2O)_4(L)]^{2+}$ L=CPO, motif II	OC–U	0.068	0.294
$[UO_2(H_2O)_3(L)]^{2+}$ L=CPO, motif III	OP–U	0.062	0.258
	OC–U	0.066	0.279

OP and OC denote the phosphoryl and carbonyl oxygen atoms

4 Conclusion

In this study, we examined the geometrical and electronic structures, and the thermodynamic stabilities of uranyl complexes with CPO or PhCPO using DFT calculation methods. When CPO/PhCPO serves as a monodentate ligand, UO_2^{2+} interacts with the OP atom, indicating that the electron-donating ability of OP is stronger than that of the OC atom. However, when CPO acts as a bidentate ligand, the U–OC bond plays a leading role in the interaction between UO_2^{2+} and CPO/PhCPO. This may be caused by the significant charge transfer from the U–OC bond orbital to the C–N antibond orbital. Additionally, the uranium character of the U–OC bond is stronger than that of the U–OP bond, and the U–OC bond shows a higher degree of covalent character. However, for $[UO_2(H_2O)_3(DL)]^{2+}$ (DL=DCPO/DPhCPO), the U–OP bonds play a leading role in the interaction between UO_2^{2+} and DCPO/DPhCPO, because the deprotonation of CPO/PhCPO causes more electrons to gather at the phosphoryl group resulting in stronger bonds between U and the phosphoryl

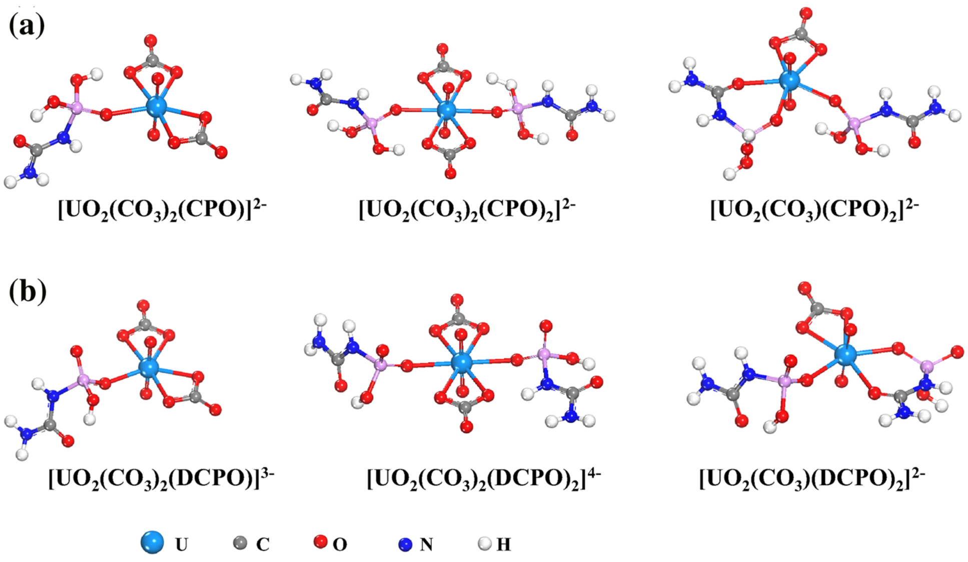

Fig. 5 (Color online) Optimized structures of most energetically stable, **a** $[UO_2(CO_3)_2(CPO)]^{2-}$, $[UO_2(CO_3)_2(CPO)_2]^{2-}$, and $[UO_2(CO_3)(CPO)_2]^{2-}$ and **b** $[UO_2(CO_3)_2(DCPO)]^{3-}$, $[UO_2(CO_3)_2(DCPO)_2]^{4-}$, and $[UO_2(CO_3)(DCPO)_2]^{2-}$

Table 11 Calculated changes in Gibbs free energies (ΔG, kcal/mol) that accompany the formation of $[UO_2(CO_3)_2(CPO)]^{2-}$, $[UO_2(CO_3)_2(CPO)_2]^{2-}$, $[UO_2(CO_3)(CPO)_2]^{2-}$, $[UO_2(CO_3)_2(DCPO)]^{3-}$, $[UO_2(CO_3)_2(DCPO)_2]^{4-}$, and $[UO_2(CO_3)(DCPO)_2]^{2-}$ at 298.15 K

Reactions	ΔG
$[UO_2(CO_3)_3]^{4-}$ + CPO → $[UO_2(CO_3)_2(CPO)]^{2-}$ + CO_3^{2-}	13.8
$[UO_2(CO_3)_2(CPO)]^{2-}$ + CPO → $[UO_2(CO_3)_2(CPO)_2]^{2-}$	9.5
$[UO_2(CO_3)_2(CPO)]^{2-}$ + CPO → $[UO_2(CO_3)(CPO)_2]^{2-}$ +CO_3^{2-}	35.0
$[UO_2(CO_3)_3]^{4-}$ + CPO → $[UO_2(CO_3)_2(DCPO)]^{3-}$ + HCO_3^{-}	− 13.8
$[UO_2(CO_3)_2(DCPO)]^{3-}$ + CPO + H_2O → $[UO_2(CO_3)_2(DCPO)_2]^{4-}$ +H_3O^{+}	47.5
$[UO_2(CO_3)_2(DCPO)]^{3-}$ + CPO → $[UO_2(CO_3)(DCPO)_2]^{2-}$ + HCO_3^{-}	− 8.3

oxygen atoms of DCPO/DPhCPO. The deprotonated CPO/PhCPO shows a higher affinity for UO_2^{2+} than the neutral CPO/PhCPO as expected. According to the ΔG values, the bidentate binding motif is favored over the monodentate binding motif for uranyl complexes with CPO/PhCPO. Anchoring a phenyl substituent at the terminal nitrogen atom of CPO exerts a slightly negative effect on the interaction between UO_2^{2+} and PhCPO. The entropy exerts a positive effect on the interaction between UO_2^{2+} and CPO/PhCPO if CPO/PhCPO acts as a bidentate ligand. However, if CPO/PhCPO serves as a monodentate ligand, the entropy exerts a negative effect.

References

1. M. Carboni, C.W. Abney, S. Liu et al., Highly porous and stable metal-organic frameworks for uranium extraction. Chem. Sci. **4**, 2396–2402 (2013). https://doi.org/10.1039/C3SC50230A
2. OECD/IAEA, Uranium 2011: Resources, Production and Demand. OECD Publishing. **2012**, 1–489 (2012)
3. N. F. Lane, Powerful Partnerships: The Federal Role in International Cooperation on Energy Innovation, Office of the President of the United States (1999)
4. L.R. Morss, N.M. Edelstein, J. Fuger et al., *The Chemistry of the Actinide and Transactinide Elements* (Springer, Dordrecht, 2006), pp. 1893–2012
5. M. Sawicki, J.-M. Siaugue, C. Jacopin et al., Discovery of powerful uranyl ligands from efficient synthesis and screening. Chemi-Eur. J. **11**, 3689–3697 (2005). https://doi.org/10.1002/chem.200401056
6. M. Sawicki, D. Lecerclé, G. Grillon et al., Bisphosphonate sequestering agents. Synthesis and preliminary evaluation for in vitro and in vivo uranium(VI) chelation. Eur. J. Med. Chem. **43**, 2768–2777 (2008). https://doi.org/10.1016/j.ejmech.2008.01.018
7. S.D. Alexandratos, X. Zhu, High-affinity ion-complexing polymer-supported reagents: immobilized phosphate ligands and their affinity for the uranyl ion. React. Funct. Polym. **67**, 375–382 (2007). https://doi.org/10.1016/j.reactfunctpolym.2007.01.013
8. L.-Y. Yuan, Y.-L. Liu, W.-Q. Shi et al., High performance of phosphonate-functionalized mesoporous silica for U(vi) sorption from aqueous solution. Dalton. T. **40**, 7446–7453 (2011). https://doi.org/10.1039/c1dt10085h
9. M. Carboni, C.W. Abney, K.M.L. Taylor-Pashow et al., Uranium sorption with functionalized mesoporous carbon materials. Ind. Eng. Chem. Res. **52**, 15187–15197 (2013). https://doi.org/10.1021/ie402646r

10. J.L. Vivero-Escoto, M. Carboni, C.W. Abney et al., Organo-functionalized mesoporous silicas for efficient uranium extraction. Micropor. Mesopor. Mat. **180**, 22–31 (2013). https://doi.org/10.1016/j.micromeso.2013.05.030
11. E. Philip Horwitz, D.C. Kalina, H. Diamond et al., The truex process-a process for the extraction of the tkansuranic elements erom nitric AC in wastes utilizing modified purex solvent. Solvent. Extr. Ion. Exc. **3**, 75–109 (1985). https://doi.org/10.1080/07366298508918504
12. S. Alegret, Developments in solvent extraction. Published for the Institut d'Estudis Catalans, Barcelona by E. Horwood (1988)
13. C.-Z. Wang, J.-H. Lan, Y.-L. Zhao et al., Density functional theory studies of UO_2^{2+} and NpO_2^+ complexes with carbamoylmethylphosphine oxide ligands. Inorg. Chem. **52**, 196–203 (2013). https://doi.org/10.1021/ic301592f
14. E.I. Matrosov, E.I. Goryunov, T.V. Baulina et al., First complexes of N-diphenylphosphorylureas with actinides and lanthanides: synthesis and structure. Dokl. Chem. **432**, 136–139 (2010). https://doi.org/10.1134/S0012500810050058
15. I.G. Tananaev, A.A. Letyushov, A.M. Safiulina et al., Search strategy for new efficient organophosphorus extractants for concentrating radionuclides. Dokl. Chem. **422**, 260–264 (2008)
16. M. J. Frisch, G. W. Trucks, H. B. Schlegel et al., Gaussian 09, Revision C.01. In Wallingford CT (2009). https://doi.org/10.1134/s0012500808100054
17. A.D. Becke, Density-functional exchange-energy approximation with correct asymptotic behavior. Phys. Rev. A **38**, 3098–3100 (1988)
18. C. Lee, W. Yang, R.G. Parr et al., Development of the Colle-Salvetti correlation-energy formula into a functional of the electron density. Phys. Rev. B **37**, 785–789 (1988). https://doi.org/10.1103/PhysRevB.37.785
19. W. Küchle, M. Dolg, H. Stoll et al., Ab initio pseudopotentials for Hg through Rn. Mol. Phys. **74**, 1245–1263 (1991). https://doi.org/10.1080/00268979100102941
20. M. Dolg, H. Stoll, H. Preuss et al., Relativistic and correlation effects for element 105 (hahnium, Ha): a comparative study of M and MO (M=Nb, Ta, Ha) using energy-adjusted ab initio pseudopotentials. J. Phys. Chem. **97**, 5852–5859 (1993). https://doi.org/10.1021/j100124a012
21. W. Küchle, M. Dolg, H. Stoll et al., Energy-adjusted pseudopotentials for the actinides. Parameter sets and test calculations for thorium and thorium monoxide. J. Chem. Phys. **100**, 7535–7542 (1994). https://doi.org/10.1063/1.466847
22. S. Tsushima, T. Reich, A theoretical study of uranyl hydroxide monomeric and dimeric complexes. Chem. Phys. Lett. **347**, 127–132 (2001). https://doi.org/10.1016/S0009-2614(01)01024-7
23. N. Ismail, J.-L. Heully, T. Saue et al., Theoretical studies of the actinides: method calibration for the UO_2^{2+} and PuO_2^{2+} ions. Chem. Phys. Lett. **300**, 296–302 (1999). https://doi.org/10.1016/S0009-2614(98)01394-3
24. V. Vetere, P. Maldivi, C. Adamo, Comparative studies of quasi-relativistic density functional methods for the description of lanthanide and actinide complexes. J. Comput. Chem. **24**, 850–858 (2003). https://doi.org/10.1016/S0009-2614(98)01394-3
25. E. Di Santo, M. Santos, M.C. Michelini et al., Gas-phase reactions of the bare Th^{2+} and U^{2+} ions with small alkanes, CH_4, C_2H_6, and C_3H_8: experimental and theoretical study of elementary organoactinide chemistry. J. Am. Chem. Soc. **133**, 1955–1970 (2011). https://doi.org/10.1021/ja109621n
26. X. Guo, X.-G. Xiong, C. Li et al., DFT investigations of uranium complexation with amidoxime-, carboxyl- and mixed amidoxime/carboxyl-based host architectures for sequestering uranium from seawater. Inorg. Chim. Acta **441**, 117–125 (2016). https://doi.org/10.1016/j.ica.2015.11.013
27. X. Guo, L. Huang, C. Li et al., Sequestering uranium from $UO_2(CO_3)_3^{4-}$ in seawater with amine ligands: density functional theory calculations. Phys. Chem. Chem. Phys. **17**, 14662–14673 (2015). https://doi.org/10.1039/c5cp00931f
28. A. Klamt, G. Schuurmann, COSMO: a new approach to dielectric screening in solvents with explicit expressions for the screening energy and its gradient. J. Chem. Soc. Perkin. Trans. **2**(5), 799–805 (1993). https://doi.org/10.1039/P29930000799
29. C.C. Pye, T. Ziegler, An implementation of the conductor-like screening model of solvation within the Amsterdam density functional package. Theor. Chem. Acc. **101**, 396–408 (1999). https://doi.org/10.1007/s00214990m184
30. J.P. Foster, F. Weinhold, Natural hybrid orbitals. J. Am. Chem. Soc. **102**, 7211–7218 (1980). https://doi.org/10.1039/C2DT30978E
31. E.D. Glendening, C.R. Landis, F. Weinhold, NBO 6.0: Natural bond orbital analysis program. J. Comput. Chem. **34**, 1429–1437 (2013). https://doi.org/10.1002/jcc.23366
32. R.F.W. Bader, Atoms in molecules. Acc. Chem. Res. **18**, 9–15 (1985). https://doi.org/10.1021/ar00109a003
33. T. Lu, F. Chen, Multiwfn: A multifunctional wavefunction analyzer. J. Comput. Chem. **33**, 580–592 (2012). https://doi.org/10.1002/jcc.22885
34. A.V. Marenich, J. Ho, M.L. Coote, Computational electrochemistry: prediction of liquid-phase reduction potentials. Phys. Chem. Chem. Phys. **16**, 15068–15106 (2014). https://doi.org/10.1039/C4CP01572J
35. A.A. Isse, A. Gennaro, Absolute potential of the standard hydrogen electrode and the problem of interconversion of potentials in different solvents. J. Phys. Chem. B **114**, 7894–7899 (2010). https://doi.org/10.1021/jp100402x
36. M.D. Tissandier, K.A. Cowen, W.Y. Feng, The proton's absolute aqueous enthalpy and Gibbs free energy of solvation from cluster-ion solvation data. J. Phys. Chem. A **102**, 7787–7794 (1998). https://doi.org/10.1021/jp982638r
37. X. Guo, Y. Wang, C. Li et al., Optimum complexation of uranyl with amidoxime in aqueous solution under different pH levels: density functional theory calculations. Mol. Phys. **113**, 1327–1336 (2015). https://doi.org/10.1080/00268976.2014.993732
38. S. Vukovic, L.A. Watson, S.O. Kang et al., How amidoximate binds the uranyl cation. Inorg. Chem. **51**, 3855–3859 (2012). https://doi.org/10.1021/ic300062s
39. Q.-Y. Wu, J.-H. Lan, C.-Z. Wang et al., Understanding the interactions of neptunium and plutonium ions with graphene oxide: scalar-relativistic DFT investigations. J. Phys. Chem. A **118**, 10273–10280 (2014). https://doi.org/10.1021/jp5069945
40. G. Tian, S.J. Teat, Z. Zhang et al., Sequestering uranium from seawater: binding strength and modes of uranyl complexes with glutarimidedioxime. Dalton. Trans. **41**, 11579–11586 (2012). https://doi.org/10.1002/jcc.22885
41. J.N. Mathur, Complexation and thermodynamics of the uranyl ion with phosphate. Polyhedron **10**, 47–53 (1991). https://doi.org/10.1002/chin.199118018
42. K.B. Wiberg, Application of the pople-santry-segal CNDO method to the cyclopropylcarbinyl and cyclobutyl cation and to bicyclobutane. Tetrahedron **24**, 1083–1096 (1968). https://doi.org/10.1016/0040-4020(68)88057-3
43. R.F.W. Bader, Atoms in molecule: a quantum theory. J. Mol. Struc-Theochem. **360**, 1–39 (1996). https://doi.org/10.1016/S0166-1280(96)90925-2